

Energy Channeling and Coupling of Neutral-beam-driven Compressional Alfven Eigenmodes to Kinetic Alfven Waves in NSTX

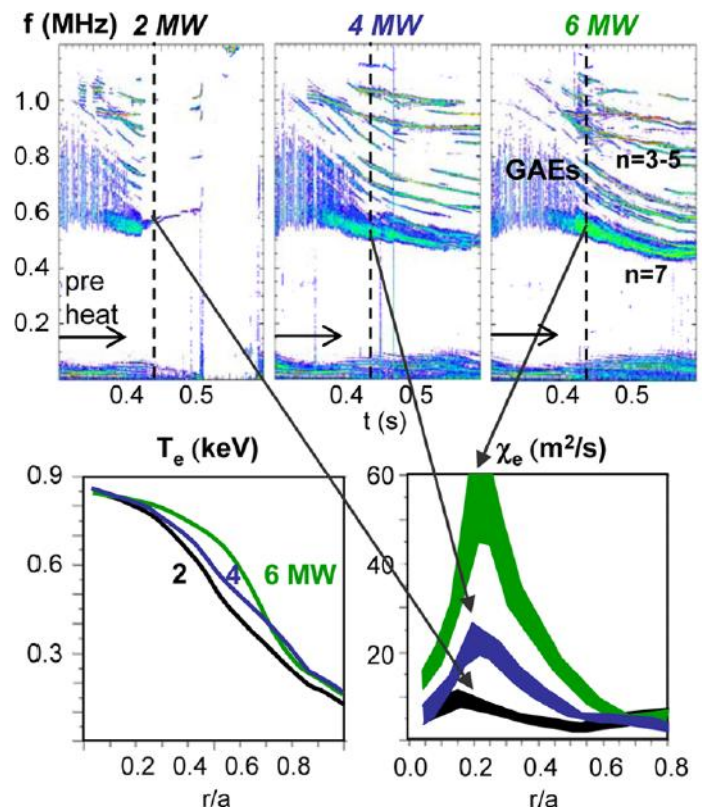
E. V. Belova (PPPL)

In collaboration with: N. N. Gorelenkov (PPPL), N. A. Crocker (UCLA), E. D. Fredrickson, and K. Tritz (PPPL)

APS DPP Meeting, New Orleans LA, October 2014

Correlation between strong GAE/CAE activity and flattening of the electron temperature profile has been observed in NSTX [Stutman, PRL 2009]

- Intense GAE/CAE activity (0.5-1.1MHz).
- Flattening of T_e profile with
 - increased beam power;
 - beam energy scanned between 60 and 90 keV [Stutman, PRL 2009].
- Was attributed to enhanced electron transport.
 - Test particle simulations predict thermal electron transport due to orbit stochasticity in the presence of multiple GAEs [Gorelenkov, NF 2010].
- Different mechanism is considered here: Energy channeling due to coupling to KAW.
- Anomalously low T_e potentially can have significant implications for future fusion devices, especially low aspect ratio tokamaks.



Correlation between GAE activity, T_e flattening, and central electron heat diffusivity χ_e in NSTX H modes with 2, 4, and 6MW neutral beam.

HYM – Parallel Hybrid/MHD Code

HYM code developed at PPPL and used to investigate kinetic effects on MHD modes in toroidal geometry (FRCs and NSTX)

- 3-D nonlinear, parallel.
- Several different physical models:
 - Resistive MHD & Hall-MHD.
 - Hybrid (fluid electrons, particle ions).
 - MHD/particle (one-fluid thermal plasma, + energetic particle ions).
- Full-orbit kinetic ions.
- Delta-f numerical scheme.
- Production size run: 5-20 wall clock hours.

Self-consistent MHD + fast ions coupling scheme

Background plasma - fluid:

$$\rho \frac{d\mathbf{V}}{dt} = -\nabla p + (\mathbf{j} - \mathbf{j}_b) \times \mathbf{B} - n_b (\mathbf{E} - \eta \mathbf{j})$$

$$\mathbf{E} = -\mathbf{V} \times \mathbf{B} + \eta \mathbf{j}$$

$$\mathbf{B} = \mathbf{B}_0 + \nabla \times \mathbf{A}$$

$$\partial \mathbf{A} / \partial t = -\mathbf{E}$$

$$\mathbf{j} = \nabla \times \mathbf{B}$$

$$\partial p^{1/\gamma} / \partial t = -\nabla \cdot (\mathbf{V} p^{1/\gamma})$$

$$\partial \rho / \partial t = -\nabla \cdot (\mathbf{V} \rho)$$

Fast ions – delta-F scheme:

$$\frac{d\mathbf{x}}{dt} = \mathbf{v}$$

$$\frac{d\mathbf{v}}{dt} = \mathbf{E} - \eta \mathbf{j} + \mathbf{v} \times \mathbf{B}$$

$$w = \delta F / F \quad \text{- particle weight}$$

$$\frac{dw}{dt} = -(1-w) \frac{d(\ln F_0)}{dt}$$

$$F_0 = F_0(\varepsilon, \mu, p_\phi)$$

ρ , \mathbf{V} and p are thermal plasma density, velocity and pressure, n_b and \mathbf{j}_b are beam ion density and current, and $n_b \ll n_e$ – is assumed.

Self-consistent anisotropic equilibrium including the NBI ions

Grad-Shafranov equation for two-component plasma:

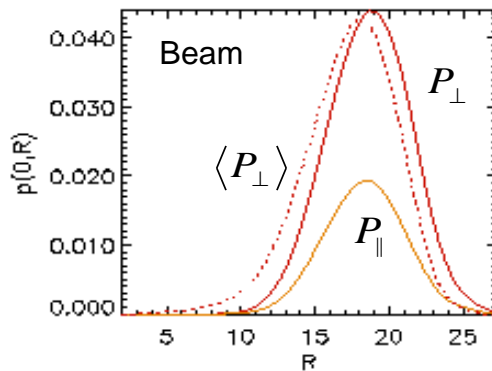
MHD plasma (thermal) and fast ions [Belova et al, Phys. Plasmas 2003].

$$\frac{\partial^2 \psi}{\partial z^2} + R \frac{\partial}{\partial R} \left(\frac{1}{R} \frac{\partial \psi}{\partial R} \right) = -R^2 p' - HH' - \underbrace{GH' + RJ_{b\phi}}_{\text{Beam effects}}$$

$$\mathbf{B} = \nabla \phi \times \nabla \psi + h \nabla \phi$$

$$h(R, z) = H(\psi) + G(R, z)$$

$$\mathbf{J}_{bp} = \nabla G \times \nabla \phi, \quad G - \text{poloidal stream function}$$



Modifications of equilibrium due to beam ions:

- more peaked current profile,
 - anisotropic pressure,
 - increase in Shafranov shift
- might have indirect effect on stability.

Fast ions – delta-f scheme: $F_0 = F_0(\varepsilon, \mu, p_\phi)$

Equilibrium distribution function $F_0 = F_1(v) F_2(\lambda) F_3(p_\phi, v)$

$$F_1(v) = \frac{1}{v^3 + v_*^3}, \text{ for } v < v_0$$

$$F_2(\lambda) = \exp(-(\lambda - \lambda_0)^2 / \Delta\lambda^2)$$

$$F_3(p_\phi, v) = \frac{(p_\phi - p_0)^\beta}{(R_0 v - \psi_0 - p_0)^\beta}, \text{ for } p_\phi > p_0$$

where $v_0 = 2-5v_A$, $v_* = v_0/2$, $\lambda = \mu B_0 / \varepsilon$ – pitch angle parameter, $\lambda_0 = 0.5-0.7$, and $\mu = \mu_0 + \mu_1$ includes first-order corrections [Littlejohn'81]:

$$\mu = \frac{(\mathbf{v}_\perp - \mathbf{v}_d)^2}{2B} - \frac{\mu_0 v_\parallel}{2B} [\hat{\mathbf{b}} \cdot \nabla \times \hat{\mathbf{b}} - 2(\hat{\mathbf{a}} \cdot \nabla \hat{\mathbf{b}}) \cdot \hat{\mathbf{c}}]$$

\mathbf{v}_d is magnetic gradient and curvature drift velocity, $\hat{\mathbf{c}} = \mathbf{v}_\perp / v_\perp$, $\hat{\mathbf{a}} = \hat{\mathbf{b}} \times \hat{\mathbf{c}}$.

Parameters are chosen to match TRANSP beam profiles.

HYM simulations reproduce frequency range of unstable GAE and CAE modes observed in NSTX

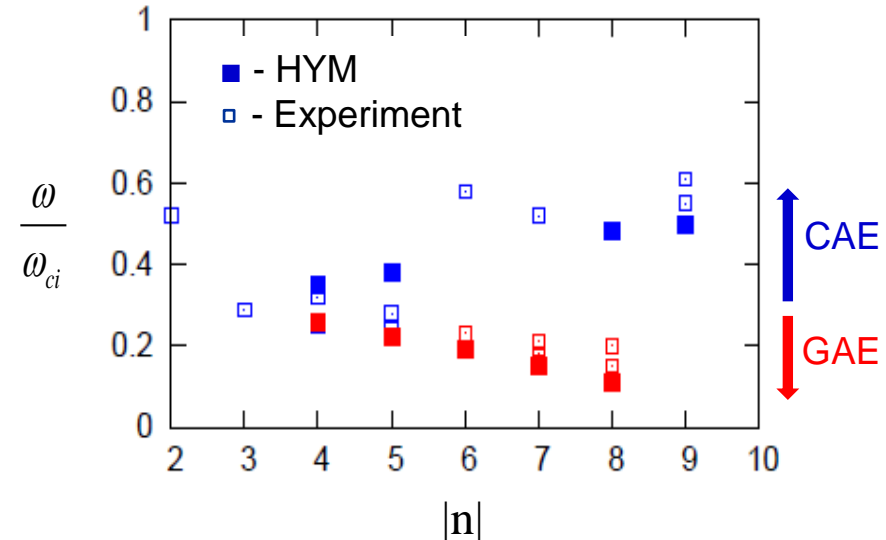
Experimental analysis:

Detailed measurements of GAE and CAE amplitudes and mode structure for H-mode plasma in NSTX shot 141398 [N. Crocker, NF 2013].

- **CAEs**: $f > 600$ kHz, and $|n| \leq 5$.
- **GAEs**: $f < 600$ kHz, and $|n| \sim 6-8$.
- Co- and counter-rotating CAEs with $f \sim 1.2-1.8$ MHz, and $n=6-14$ also observed in the same shot [E. Fredrickson, PoP 2013].

HYM simulations:

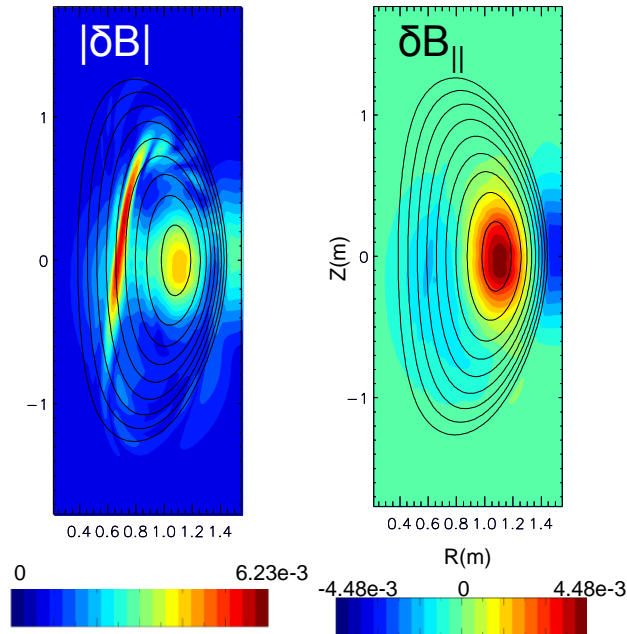
- For $n=5-7$ most unstable are counter-rotating **GAEs**, with $f = 380-550$ kHz.
- For $n=4$ and $n=8, 9$ most unstable are co-rotating **CAEs** with $f = 870-1200$ kHz.



Frequency versus toroidal mode number for unstable GAEs (red) and CAEs (blue), from HYM simulations and experiment, $f_{ci} = 2.5$ MHz.

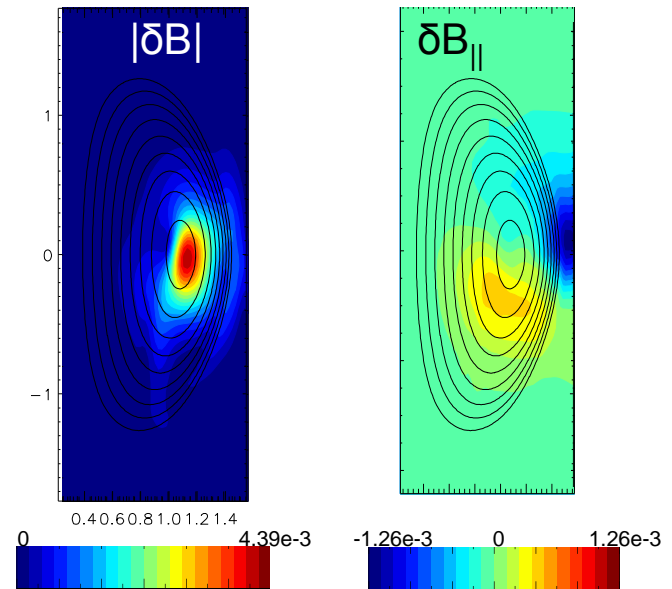
CAE has large compressional component in the core and couples to KAW

$n=4$, CAE



$\delta B_{||}$ is significantly larger than δB_{\perp} at the axis.

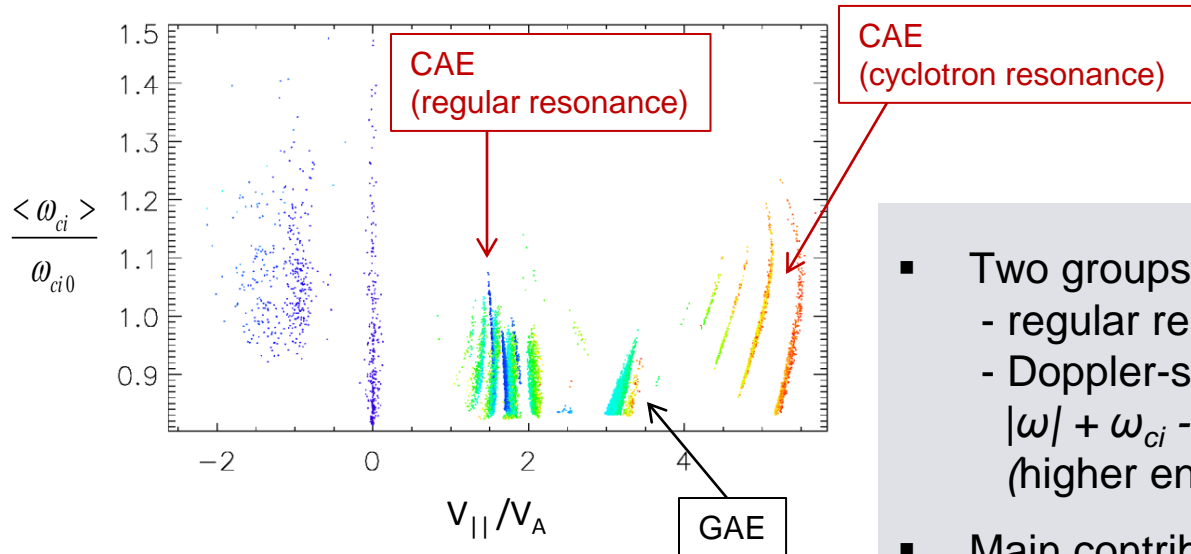
$n=6$, GAE



$\delta B_{||}$ is comparable to δB_{\perp} only at the edge.

- CAE/KAW coupling seen for all unstable CAEs.
- KAW has large amplitude on HFS.

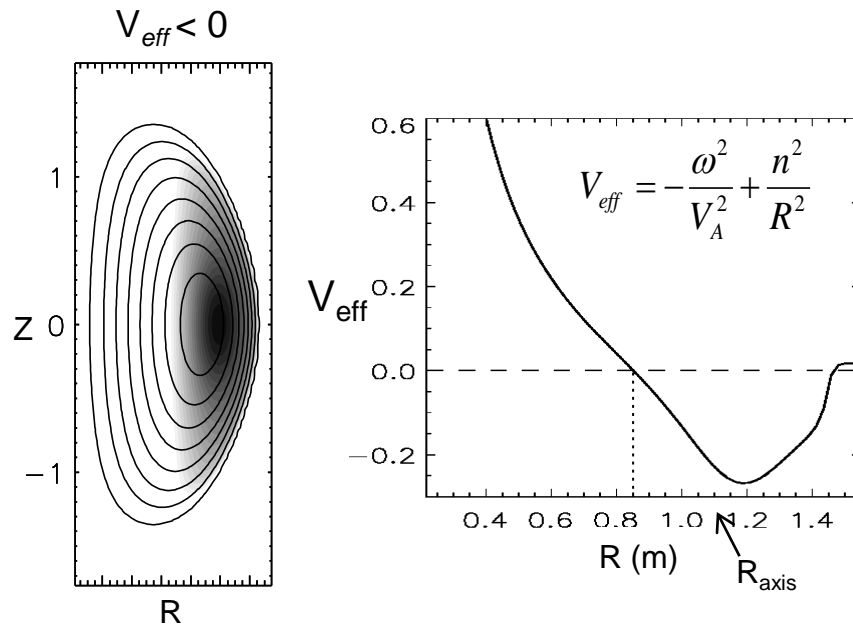
Simulations: main drive for CAE comes from resonant particles with $v_{||} \sim \omega/k_{||}$



Orbit-averaged cyclotron frequency vs orbit-averaged parallel velocity for resonant particles. From simulations for $n=8$ CAE ($\omega=0.48\omega_{ci0}$, $\gamma=0.004\omega_{ci0}$). Particle color corresponds to different energies: from $E=0$ (purple) to $E=90\text{keV}$ (red).

- Two groups of resonant particles:
 - regular resonance: $\omega - k_{||}v_{||} = 0$,
 - Doppler-shifted cyclotron resonance: $|\omega| + \omega_{ci} - k_{||}v_{||} = 0$ (higher energy particles).
- Main contribution comes from the beam ions with $v_{||} \sim \omega/k_{||}$.
- “Turning off” high-energy resonant particles does not change the growth rate \rightarrow contribution from the cyclotron resonances is negligible.

CAE/KAW coupling is universal



Contour plot and radial profile of the effective potential V_{eff} for $n=8$ CAE mode with $\omega=0.48\omega_{ci0}$. Mode can exist for $V_{eff} < 0$ with radial extent: $0.85 < R < 1.45$ m.

Approximate equation for CAE mode, assuming circular cross-section, and neglecting beam effects and coupling to SAW:

$$\frac{\partial^2 \delta B_{\parallel}}{\partial r^2} = V_{eff} \delta B_{\parallel}$$

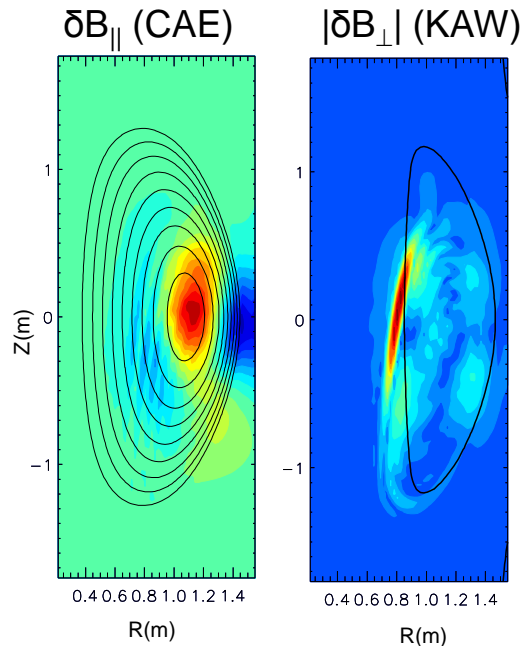
$$V_{eff} = -\frac{\omega^2}{V_A^2} + k_{\parallel}^2$$

HYM simulations show unstable $n=8$ mode with $\omega=0.48\omega_{ci0}$ and $\gamma=0.004\omega_{ci0}$.

Effective potential well for $n=8$ mode is narrower and deeper than V_{eff} for $n=4$ resulting in more localized CAE mode with larger frequency.

Edge of CAE well coincides with resonance location \rightarrow CAE/KAW coupling.

On-axis CAE couples to off-axis KAW



Magnetic field perturbation for $n=8$ co-rotating CAE.
Solid line corresponds to $\omega_A(Z,R)=\omega$.

$n=8$ co-rotating CAE shows resonant coupling to KAW.

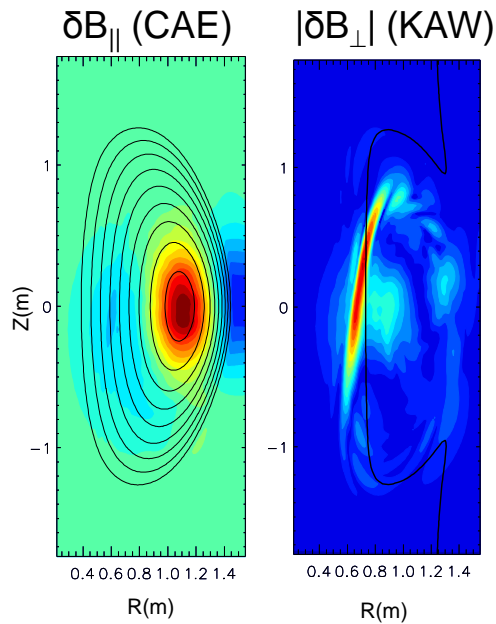
CAE peaks near magnetic axis, where $\delta B_{||} \gg \delta B_{\perp}$, KAW is located at the resonance ω_A (Z,R)= ω on HFS.

KAW structure is tilted relative to equilibrium magnetic field:

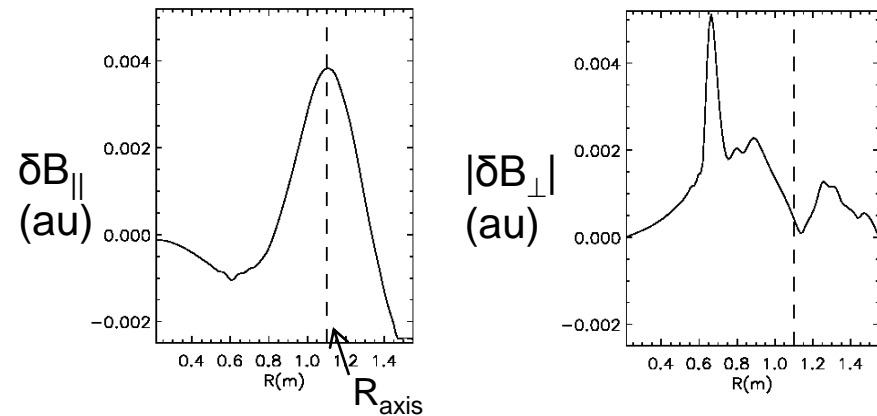
- $\mathbf{k}_{||}$ is in the direction of the beam velocity
- \mathbf{k}_{\perp} directed towards high-density side
- $k_{\perp} \gg k_{||}$

This results in a mode structure which is not symmetric relative to mid-plane.

KAW amplitude is larger than amplitude of driving CAE mode



Magnetic field perturbation for $n=4$ co-rotating CAE. Solid line corresponds to $\omega_A(Z,R)=\omega$.



Radial profiles of magnetic field perturbation for the $n=4$ CAE versus major radius.

At the KAW resonance location the amplitude of KAW is larger than the amplitude of driving CAE mode.

Scale-length for beam-KAW is the beam ion Larmor radius.

KAW dispersion relation - assuming three-component plasma, Maxwellian ions with $V_0=0$, and including only adiabatic beam ions response (non-perturbative).

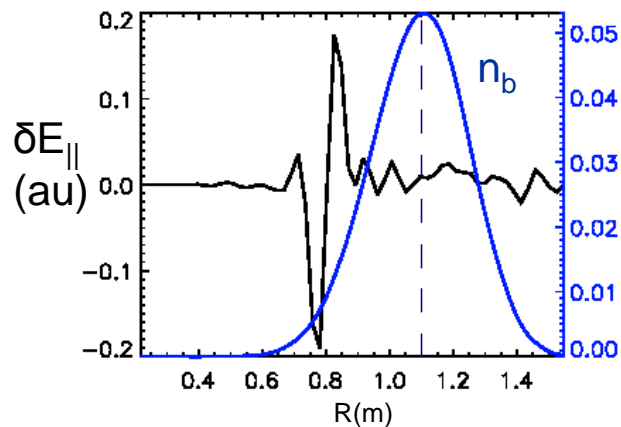
$$\text{KAW in full kinetic model: } \omega^2 = k_{\parallel}^2 V_A^2 \left(1 + \lambda_e + \frac{3 n_i}{4 n_e} \lambda_i + \frac{3 n_b}{4 n_e} \lambda_b - \frac{\omega^2}{\omega_{ci}^2} \right),$$

$$\text{where } \lambda_{\alpha} = \frac{k_{\perp}^2 T_{\alpha}}{m_i \omega_{ci}^2}$$

$$\text{KAW in HYM model: } \omega^2 = k_{\parallel}^2 V_A^2 \left(1 + \frac{3 n_b}{4 n_e} \lambda_b - \frac{n_b}{n_e} \frac{\omega^2}{\omega_{ci}^2} \right), \quad \lambda_b = \frac{k_{\perp}^2 T_b}{m_i \omega_{ci}^2}$$

- consistent with full kinetic in the limit $\lambda_e \rightarrow 0$, $\lambda_i \rightarrow 0$, and $\omega \ll \omega_{ci}$.

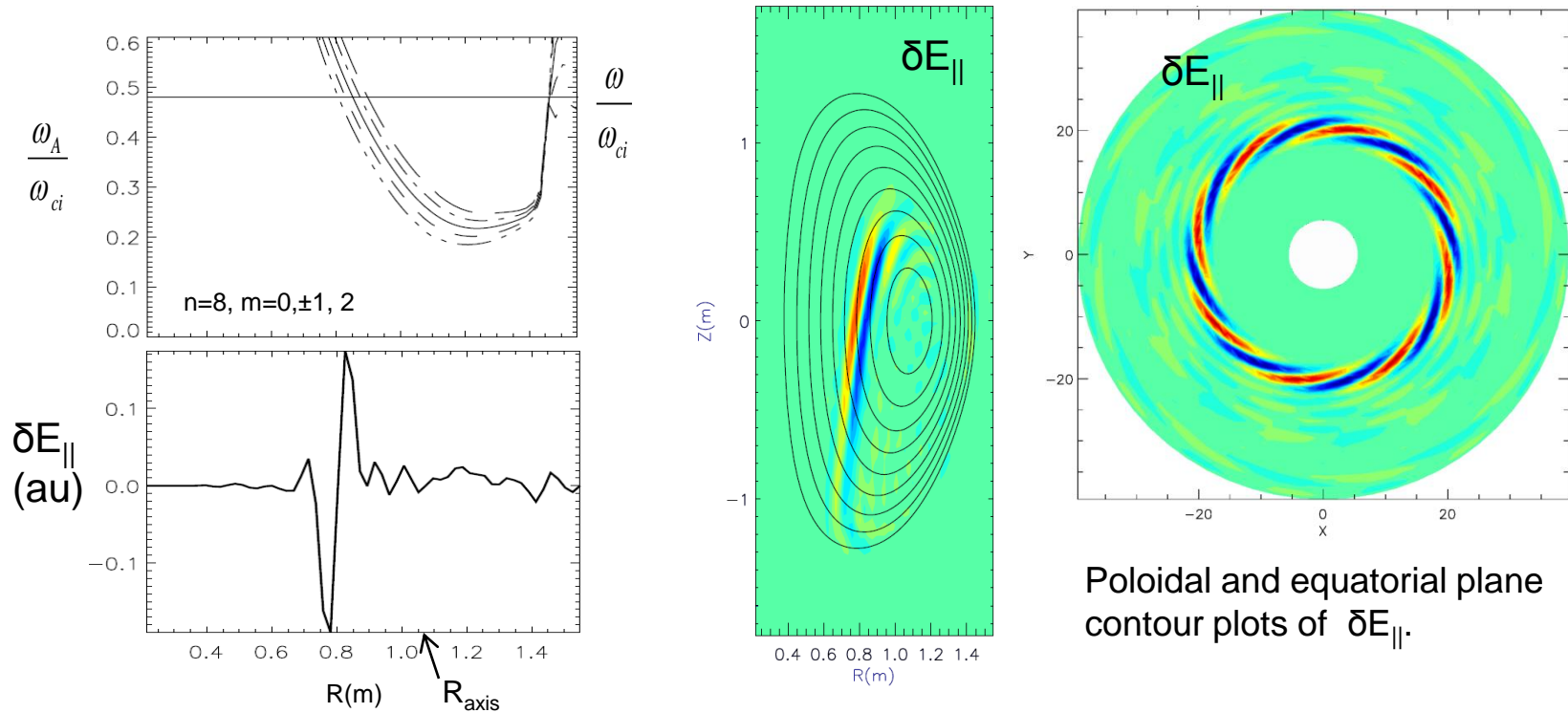
Resonance with KAW is located near the edge of beam



Radial profiles of δE_{\parallel} for $n=8$ CAE/KAW and beam ion density.

- Radial width of KAW is comparable to beam ions Larmor radius, $k_{\perp} \rho_{\text{beam}} \sim 1$.
- Resonant mode polarization is consistent with KAW mode, ie $\delta B_Z \gg \delta B_R, \delta B_{\parallel}$ and $\delta V_Z \gg \delta V_R, \delta V_{\parallel}$ with $\delta V_Z \sim -\delta B_Z$.
- Resonance with KAW is located at the edge of CAE well, near the edge beam ion density profile at $r/a \sim 0.6$.

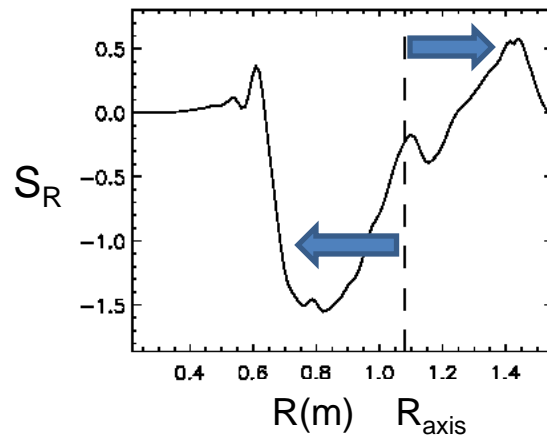
Low-n and high-n CAE modes show coupling to KAW



Radial profiles of Alfvén continuum and $\delta E_{||}$ for $n=8$.

KAW can have strong effect on electron transport due to finite $\delta E_{||}$.

Relation between CAE/KAW and T_e flattening?



Radial component of quasilinear Poynting vector $\mathbf{S} = \langle \mathbf{E} \times \mathbf{B} \rangle$.
Energy flux is directed away from magnetic axis, ie from CAE to KAW.

Fraction of NBI power transferred to CAE:

$$P = 2\gamma \int (\delta B)^2 / 4\pi d^3x,$$

$\delta B/B_0 = (0.9-3.4) \times 10^{-3}$ corresponds to measured displacement $|\xi| = 0.1-0.4$ mm [N.Crocker'13] (based on HYM-calculated mode structure for $n=4$ CAE).

For $\gamma/\omega_{ci} = 0.005-0.01 \rightarrow \mathbf{P} = (0.013 - 0.4) \text{ MW}$,

- significant fraction of NBI energy can be transferred to several unstable CAEs of relatively large amplitudes.

Energy flux from the CAE to the KAW and dissipation at the resonance location can have a strong effect on T_e profile.

CAE/KAW coupling can provide an efficient energy channeling mechanism, and can have direct effect on the T_e profiles.

- Simulations show unstable CAE modes for toroidal mode numbers $n=4-9$ in H-mode NSTX discharges.
- Unstable CAE modes couple with KAW on the HFS. Resonance with KAW is located at the edge of CAE well, and just inside beam ion density profile. Radial width of KAW is comparable to beam ion Larmor radius.
- A significant fraction of NBI energy can be transferred to several unstable CAEs: up to $P \sim 0.4 \text{ MW}$ for one mode with $\delta B/B_0 \sim 10^{-3}$.
- Energy flux is shown to be directed away from the magnetic axis (CAE) toward the resonance location (KAW).
- Strong CAE/KAW coupling follows from dispersion relation, therefore, this mechanism applies to any device with unstable CAEs.
- Detailed comparison of the relative importance of the energy channeling and anomalous electron transport mechanisms will require fully nonlinear simulations, and will be performed in the future.